Biogeosciences, 16, 275–288, 2019
https://doi.org/10.5194/bg-16-275-2019

Biogeosciences Open Access EGU

Varying relationships between fire radiative power and fire size at a global scale

Pierre Laurent[1], **Florent Mouillot**[2], **Maria Vanesa Moreno**[2], **Chao Yue**[3], **and Philippe Ciais**[1]

[1]Laboratoire des Sciences du Climat et de l'Environnement (LSCE), CEA-CNRS-UVSQ, UMR8212, Gif-sur-Yvette, France
[2]UMR CEFE 5175, Centre National de la Recherche Scientifique (CNRS), Université de Montpellier, Université Paul-Valéry Montpellier, Ecole Pratique des Hautes Etudes (EPHE), Institut de Recherche pour le Développement, 1919 route de Mende, 34293 Montpellier CEDEX 5, France
[3]State Key Laboratory of Soil Erosion and Dryland Farming on the Loess Plateau, Northwest A&F University, Yangling, Shaanxi 712100, China

Correspondence: Pierre Laurent (pierre.laurent@lsce.ipsl.fr) and Florent Mouillot (florent.mouillot@ird.fr)

Received: 10 July 2018 – Discussion started: 23 August 2018
Revised: 8 December 2018 – Accepted: 24 December 2018 – Published: 22 January 2019

Abstract. Vegetation fires are an important process in the Earth system. Fire intensity locally impacts fuel consumption, damage to the vegetation, chemical composition of fire emissions and also how fires spread across landscapes. It has been observed that fire occurrence, defined as the frequency of active fires detected by the MODIS sensor, is related to intensity with a hump-shaped empirical relation, meaning that occurrence reaches a maximum at intermediate fire intensity. Raw burned area products obtained from remote sensing can not discriminate between ignition and propagation processes. To go beyond burned area and to test if fire size is driven by fire intensity at a global scale as expected from empirical fire spread models, we used the newly delivered global FRY database, which provides fire patch functional traits based on satellite observation, including fire patch size, and the fire radiative power measures from the MCD14ML dataset. This paper describes the varying relationships between fire size and fire radiative power across biomes at a global scale. We show that in most fire regions of the world defined by the GFED database, the linear relationship between fire radiative power and fire patch size saturates for a threshold of intermediate-intensity fires. The value of this threshold differs from one region to another and depends on vegetation type. In the most fire-prone savanna regions, once this threshold is reached, fire size decreases for the most intense fires, which mostly happen in the late fire season. According to the percolation theory, we suggest that the decrease in fire size for more intense late season fires is a consequence of the increasing fragmentation of fuel continuity throughout the fire season and suggest that landscape-scale feedbacks should be developed in global fire modules.

1 Introduction

Fire is a major perturbation of the Earth system, which impacts the plant biomass distribution and vegetation structure, the carbon cycle, global atmospheric chemistry, air quality and climate (Bowman and Balch, 2009). Fire is therefore recognised as an essential climatic variable (GCOS, 2011), and the potential impact of global warming on drought severity and fire season length is a key scientific question (Flannigan et al., 2009; Krawchuk et al., 2009; Aragão et al., 2018) to understand its role within the Earth system. Most dynamic global vegetation models (DGVMs) have included fire modules (see Hantson et al., 2016; Rabin et al., 2017, for a review) to improve the prediction of the impact of fire on vegetation dynamics and the carbon cycle. Substantial efforts have been devoted in the past decades to create reliable global burned area (BA), active fire and fire radiative power (FRP) datasets which allow the quantification of the fire perturbation since the beginning of the 2000s (Mouillot et al., 2014) and benchmark DGVM fire modules.

A fire can be decomposed as a two-step process, the ignition and the propagation (Pyne et al., 1996; Scott et al., 2014). Potential fire ignitions are set by lightning strikes

and humans (deliberately or accidentally), and the probability that an ignition turns into a spreading fire event mainly depends on fuel type and its moisture content at the location of the ignition. The Rothermel equation (Rothermel, 1972) has long been used to model fire propagation in landscape fire succession models (Cary et al., 2006), whose rate of spread scales with a power function of the wind velocity, landscape slope and fire intensity. However, this model, used by processed-based fire modules in most DGVMs, has only been benchmarked on experimental and localised fires, discarding topographic and landscape effects. In addition, for larger natural fires, the continuity of the fuel bed also has an impact on fire propagation: a homogeneous fuel bed usually promotes fire propagation (Baker et al., 1994) while fragmented landscape with a heterogeneity of fuel patches reduces fire spread (Turner, 1989). Conversely, the velocity of fire propagation determines the amount of fuel entering the combustion zone and therefore feeds back on the intensity of the fire event. In addition to its coupling with fire propagation, fire intensity also significantly impacts the chemical composition of the emissions (Tang and Arellano, 2017), the amplitude and severity of vegetation damage, and vegetation post-fire regeneration ability (Bond and Keeley, 2005). As a result, analyses focusing on fire patch properties, such as fire patch size and shape, rather than on simple BA have emerged in the last decade. Information on the fire patch size distribution (Archibald et al., 2010; Hantson et al., 2015; Laurent et al., 2018) can be used to map the different fire regimes at a global scale (Archibald et al., 2013), and edge effects could reveal landscape-scale processes, leading to the observed shapes of burned patches (Greene et al., 2005; Cary et al., 2009).

Recent studies (Pausas and Ribeiro, 2013; Luo et al., 2017) have shown that fire occurrence, defined as the number of remotely detected active fires in units of time per unit of area, increases with fire intensity up until a threshold is reached (so-called intermediate fire occurrence–intensity (IFOI) hypothesis) above which occurrence decreases with increasing intensity. Since ignition and propagation are different processes and are not driven by the same climatic variables, it is necessary to go beyond fire occurrence and BA and to consider individual fire events. Here we document and investigate the relationship between fire patch size derived from BA data and FRP at a global scale based on remote-sensing information. FRP measures the energy emitted through radiative processes released during the combustion and can be associated with fire intensity all throughout the fire burning process (Wooster et al., 2005, 2013; Ichoku et al., 2008; Barrett and Kasischke, 2013). A positive relationship between fire patch size and the reaction intensity of the fire front is expected at least for small fire size, whose propagation rate has been benchmarked using laboratory experiments. But we do not know if this holds up at global and regional scales for bigger fires, usually reaching longer temporal scales with varying wind directions and atmospheric circulation and larger spatial extent. Fire patch size may not continue to increase with fire intensity above a certain size due to landscape fragmentation acting as a natural barrier against fire propagation. To uncover the fire size–intensity relationships, we assembled the information on fire patch size recovered from the FRY global database (Laurent et al., 2018) based on the MODIS MCD64A1 and the MERIS FireCCI41 BA products, with FRP using active fire pixel data from the MCD14ML dataset.

2 Data and methodology

We used the FRY database containing the list of fire patches characterised by their morphological traits, including fire patch size, at a global scale (Laurent et al., 2018). Fire patches were derived from the MERIS fire_cci v4.1 (later called FireCCI41; Chuvieco et al., 2016) and the MCD64A1 Collection 6 (Giglio et al., 2016) BA pixel products. The FireCCI41 product provides the pixel burn dates for the period 2005–2011 and is derived from the Envisat MERIS sensor, with a spatial resolution of $\sim 300\,\mathrm{m} \times 300\,\mathrm{m}$ and a 3-day revisit frequency at the Equator. The MCD64A1 product, derived from the MODIS sensors, provides pixel burn dates at a global scale over the period 2000–2017 with a coarser resolution ($\sim 500 \times 500\,\mathrm{m}$) but a more frequent revisit time (1 day at the Equator). The pixel burned dates are combined using a flood-fill algorithm (Archibald and Roy, 2009), which is parametrised by a cut-off value. This cut-off value corresponds to the maximum time difference between the burn date of neighbouring pixels belonging to the same fire patch. These global datasets have been thoroughly compared by the authors of the FRY database, locally compared using the US and Canadian forest service fire patch database (Chuvieco et al., 2016) and validated against Landsat fire polygons in the Brazilian Cerrado (Nogueira et al., 2017). The FRY database is organised in eight datasets (two survey times and four cut-off values) and provides for each individual fire patch a set of variables, called fire patch functional traits, including the geolocation of the patch centre, the fire patch size (later called FS, in hectares) and different indices on fire patch morphology. Standard deviation ellipses (SDEs) are fitted by Laurent et al. (2018), over each fire patch larger than 5 pixels (using the aspace R package), and the geolocation of their centres, half-axes and orientation in a longitudinal–latitudinal coordinate system, as well as the values of the minimum, mean and maximum pixel burn dates, are also provided for each fire patch.

Active fire pixel data from the MCD14ML dataset (Giglio et al., 2006) consist in a list of geographic coordinates of individual active fire pixels detected by the Terra and Aqua sensors on board the MODIS satellite for the period 2000–2017 with a resolution of $\sim 1\,\mathrm{km} \times 1\,\mathrm{km}$. For each pixel, the dataset provides the date and hour of burn of the active fire pixel, along with its FRP (in megawatts). FRP represents the energy emitted by fire through radiative processes (i.e. the

total fire intensity minus the energy dissipated through convection and conduction) over its total area. It is widely used as a proxy for fire impact assessment (Barrett and Kasischke, 2013; Sparks et al., 2018), biomass combustion rates (Roberts et al., 2005) or fire event (Hernandez et al., 2015) and fire spread (Johnson et al., 2017) modelling. We performed a spatio-temporal matching between active fire pixel data and all the fire patches from the FRY database in order to recover the average FRP for each fire patch. To do so, we consider that an active fire pixel belongs to a fire patch if it fulfils the two following conditions.

The centre of the active fire pixel must be located within the SDE of the fire patch. Since the side of an active fire pixel is 1 km, we also consider that an active fire pixel located at a distance of 1 km or less from the area covered by the SDE belongs to the fire patch.

The detection date of the active fire pixel must lie between the minimum minus a 30-day buffer and maximum burn date of the BA pixels of the fire patch. The 30-day extension is used to account for the possible time lag between the detection of an active fire pixel and its associated burned date pixels.

Once the active fire pixels belonging to each fire patch were obtained, we compute the mean FRP value of all associated pixels for each patch. The spatio-temporal matching sometimes fails to recover any active fire pixels for some fire patches. Such fire patches ($\sim 20\,\%$–$25\,\%$ of each sample) were discarded from the analysis. We observed that the number of fire patches without attributed active fire pixels increases as the cut-off decreases (see Table S1 in the Supplement). This can be explained by the fact that, for low cut-off values, a real fire event can be split by the flood-fill algorithm into different smaller fire patches. Using a shorter value for the temporal buffer (10 days) slightly increases the failure rate of the matching but had no significant impact on the results presented in this analysis.

In the following, we studied the relationship between FRP and FS in each region defined by the Global Fire Emission Database (GFED; Giglio et al., 2013, Fig. S1 in the Supplement). Since different vegetation types can occur within a GFED region (and consequently different amount of biomass or drought severity), we split all of them into three vegetation types using the GLCF MODIS Land Cover data (Channan et al., 2014) and explore the relationship between FRP and fire size for each vegetation type in each GFED region. The vegetation types are defined by grouping together MODIS Land Cover categories: "forests" stands for all the forested land cover types (evergreen or deciduous needleleaf or broadleaf forests and mixed forests), "savannas" for savannas with woody savannas, and "grasslands/shrublands" for grasslands with open and closed shrublands. The spatial extent corresponding to these three vegetation types can be found in Fig. S2 in the Supplement.

In each $1^\circ \times 1^\circ$ cell, we split the fire season into three periods: early, corresponding to the 4 months before the month with the highest BA; middle, corresponding to the peak BA month; and late fire season corresponding to the 4 months after the peak BA month. We did not split the fire patch distribution into different FRP categories because of the big asymmetry of the number of fire patches between high- and low-intensity fires. For each period, following the same methodology as in Laurent et al. (2018), we fitted a power law against the fire patch size distribution to estimate the power-law slope parameters β_{begin}, β_{middle} and β_{end}. These β parameters allow us to investigate the asymmetry of the fire size distribution in each cell. High β values imply that the size distribution is dominated by small fires.

The results presented below have been computed for each of the eight different fire patch datasets of the FRY database. However, we will further only focus on the results obtained from the MCD64A1-derived fire patch dataset, with a cut-off value of 14 days. The figures obtained for the FireCCI41 fire patch product with a cut-off of 14 days (which spans the years 2005 to 2011) can be found in the Supplement. The same analysis was also performed with a cut-off value of 3 days for both MCD64A1 and FireCCI41: testing another extreme cut-off value allows us to estimate the impact on the results of the temporal threshold parameter used to reconstruct fire patches by Laurent et al. (2018).

3 Results

The median FS and median FRP are displayed in Fig. 1. Large and intense fire patches are located in Australia, in the grasslands of Kazakhstan, in Namibia, in the Sahel and in Patagonia. High mean FRP values are also reached in South Australia, in the Mediterranean Basin, and in the forested areas of the western US and boreal North America. Conversely, fires are both smaller and less intense in croplands of North America, Europe, and South East Asia and in African savannas. The fraction of BA in the cell each year is also displayed.

The relationships between the median and 25th and 75th quantiles of FS based on MCD64A1 with a cut-off value of 14 days and FRP for different GFED regions are shown in Fig. 2. The colour of the dots and error bars represents the average of the minimum burn dates of the fire patches in each bin of FRP, and the background histograms show the number of fire patches in each FRP bin. In all GFED regions, the number of fire patches peaks at low to intermediate FRP values ($\sim$ 20–30 MW). In most GFED regions, we note that median FS and quantiles decreases once a FRP threshold is reached (Fig. 2). In order to smooth the estimation of this FRP threshold (later called FRP_{MAX}), above which FS seems to saturate, we fitted a four-degree polynomial function to the data and determined the FRP at the maximum median FS value of the fit. The results are displayed in Table 1.

Northern Hemisphere Africa (NHAF), equatorial Asia (EQAS) and South East Asia (SEAS) experience a humped relationship between FS and FRP. At low FRP

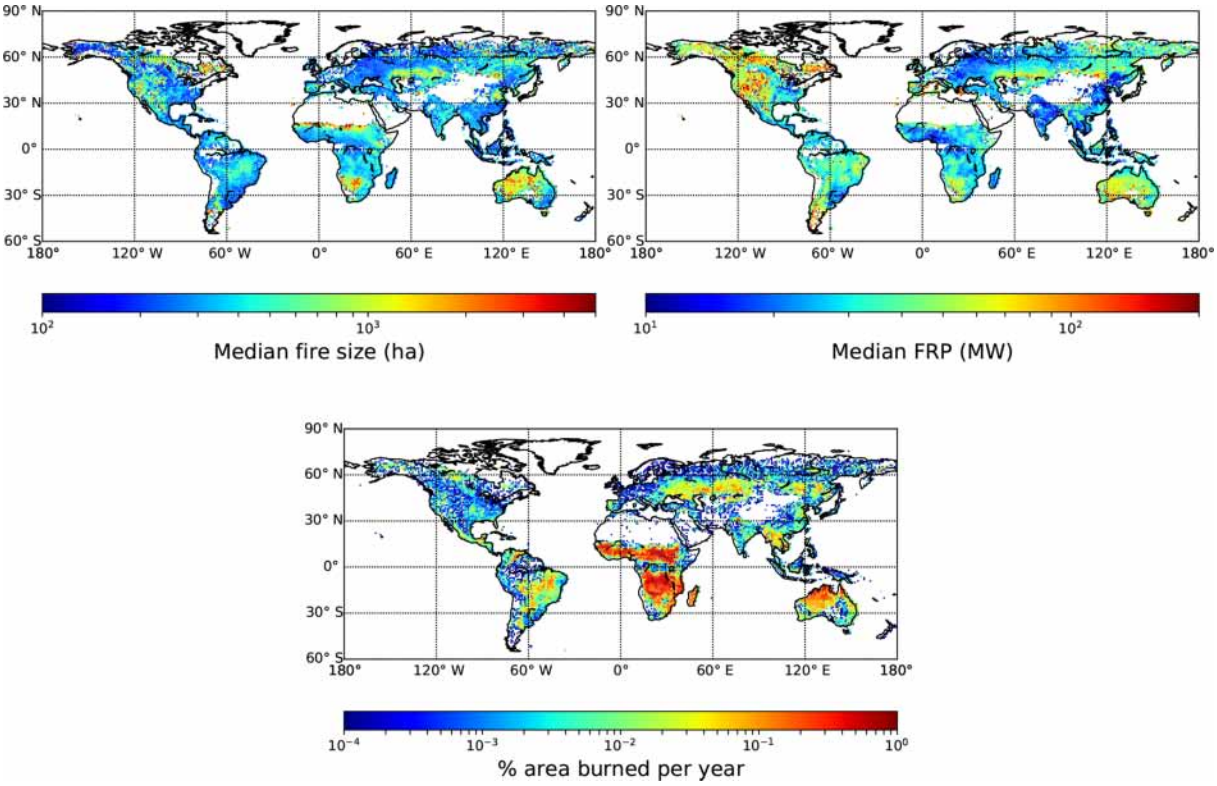

Figure 1. Median fire size (in hectares), median fire radiative power from the FRY database (derived from MCD64A1 with a cut-off of 14 days) and percentage of burned area each year (from GFED).

values (30 to 80 MW), the median and quantiles of FS increase with FRP and reach a maximum value at low to intermediate FRP (Table 1, Fig. 2). We also identified in Fig. 2 that the fire patches associated with intense fires having a FRP above the regional threshold tend to occur later in the fire season. In Central America (CEAM), Northern Hemisphere South America (NHSA), Southern Hemisphere Africa (SHAF), Southern Hemisphere South America (SHSA) and Australia (AUST), but also in boreal Asia (BOAS), the relationship between the median and quantiles of FS vs. FRP is similar. However, the maximum FS is reached at higher FRP values (from 75 to 125 MW) than for NHAF, EQAS, and SEAS, and the decrease following the maximum FS is more gradual. Intense fire events also appear later in the fire season for BOAS and AUST, and AUST exhibits the highest FS / FRP slope (9.0 ha MW^{-1} compared to 0.6 to 4.4 ha MW^{-1} for other regions). By contrast, in boreal North America (BONA), temporal North America (TENA), Europe (EURO) and central Asia (CEAS), mean FS constantly increases with FRP and only reaches a plateau at very high FRP ($\sim$ 196 MW for BONA, $\sim$ 215 MW for TENA, $\sim$ 240 MW for EURO and 277 MW for CEAS). In those temperate and boreal regions, we did not observe the humped shape relation with a decrease in FS for high FRP that occurs in other GFED regions (Fig. 2). The Middle East (MIDE) also displays a positive correlation between median FS and FRP, but the statistics for intense fire events is too low to infer any significant relationship at high FRP values.

Figure 3 displays the same analysis as Fig. 2, but each GFED region is subdivided into three vegetation types (as defined in Sect. 2), allowing an overview of the contribution of each vegetation type by region. For BONA, TENA and EURO, mostly dominated by forest fires, we observe that the generic pattern obtained in Fig. 2 is similar to the one observed for the forest vegetation type, while the other vegetation types display a more humped-shape relationship. In tropical areas (NHSA, SHSA, NHAF, SHAF, AUST), the generic pattern observed in Fig. 2 is similar to the one observed for the savanna and grassland/shrubland vegetation types, highlighting the uniform pattern in these two dominant vegetation types within the region, only differentiated by a higher median fire size for savannas. Forest vegetation types display a more linear relationship, closer to the one observed in temperate and boreal areas. In conclusion, the behaviour of the relationship between FRP and FS obtained for each GFED region is actually representative of the main dominant vegetation types composing these regions, while the non-dominant vegetation types may experience another pattern. In all regions, savanna and grassland ecosystems ex-

Table 1. Value of the FRP threshold at maximum median FS, and the slope of FS vs. FRP before the threshold value for different GFED regions. Note that the value of the decreasing slope is not always available because there is no FRP bin after the detected maximum FRP.

Vegetation type	GFED region	FRP with largest associated fire patch sizes (MW)	Slope of the FRP vs. median FS relationship before max FS (ha MW^{-1})	Slope of the FRP vs. median FS relationship after max FS (ha MW^{-1})
Savannas	BONA	175	3.907	−7.791
	TENA	221	1.179	−1.974
	CEAM	10	2.342	−0.499
	NHSA	74	2.813	−0.400
	SHSA	110	2.692	−0.661
	EURO	270	1.548	NA
	NHAF	67	5.256	−0.662
	SHAF	110	2.300	−0.172
	BOAS	224	2.149	−19.993
	CEAS	260	0.577	1.011
	SEAS	45	3.865	−0.575
	EQAS	185	1.716	2.038
	AUST	75	13.665	−1.684
Forests	BONA	220	9.204	−39.657
	TENA	222	3.404	−19.811
	CEAM	57	1.071	−0.382
	NHSA	76	1.288	−0.457
	SHSA	242	0.494	−3.859
	EURO	185	4.979	−6.128
	NHAF	68	0.609	−0.508
	SHAF	270	0.076	NA
	BOAS	88	5.734	−1.075
	CEAS	90	1.421	−0.696
	SEAS	10	3.865	−0.224
	EQAS	55	2.904	−0.395
	AUST	237	9.533	−8.085
Grasslands/shrublands	BONA	170	5.239	−1.579
	TENA	219	2.342	−2.809
	CEAM	230	2.003	−11.986
	NHSA	100	3.014	−1.451
	SHSA	148	2.700	−0.726
	MIDE	270	0.136	NA
	NHAF	220	1.329	−13.382
	SHAF	170	2.939	−2.049
	BOAS	105	5.081	−0.402
	CEAS	208	3.725	−2.341
	AUST	149	16.639	−4.785
All	BONA	196	4.420	−7.817
	TENA	215	1.359	−1.513
	CEAM	84	0.775	−0.154
	NHSA	83	2.318	−0.637
	SHSA	105	2.384	−0.237
	EURO	239	0.628	−8.143
	MIDE	198	0.553	−1.254
	NHAF	71	3.939	−0.683
	SHAF	116	2.474	−0.115
	BOAS	86	3.409	−0.346
	CEAS	277	0.613	NA
	SEAS	37	3.906	−0.327
	EQAS	60	3.112	−0.187
	AUST	142	9.169	−0.523

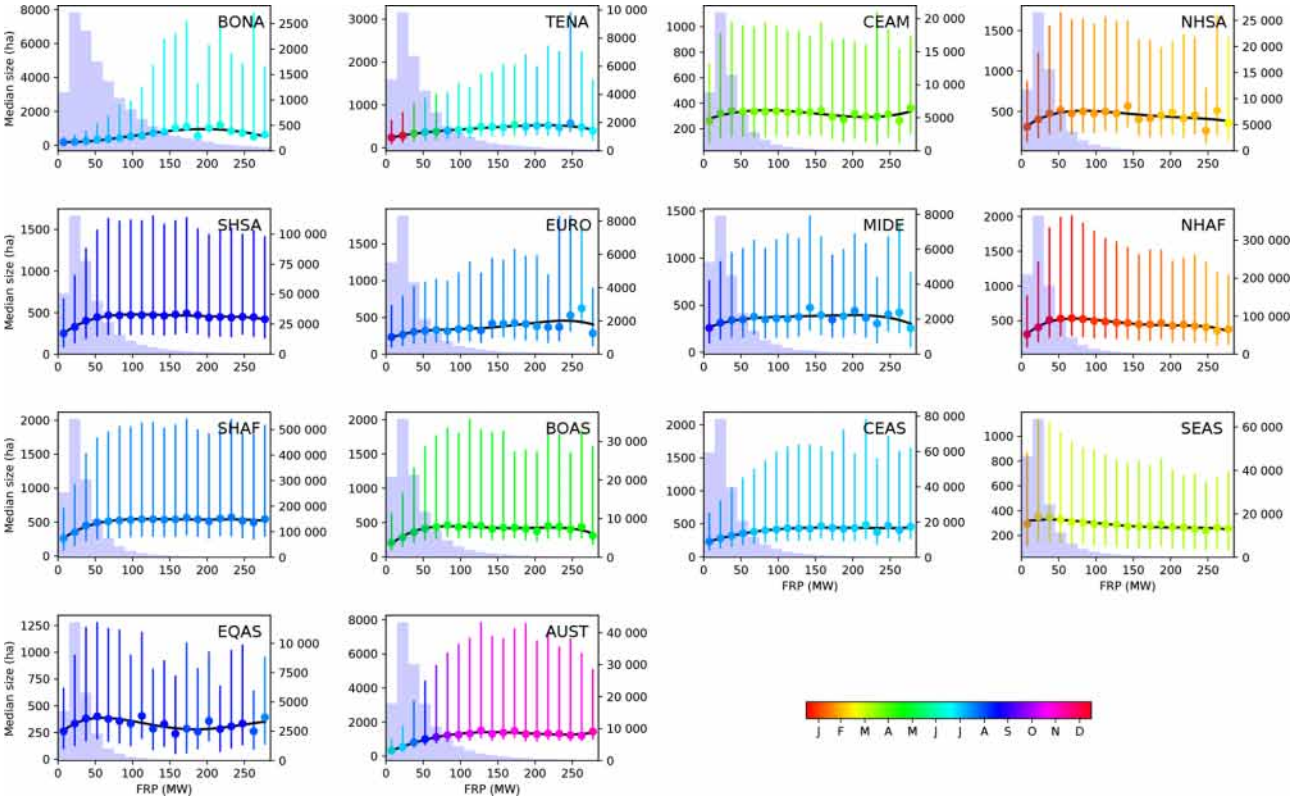

Figure 2. Median fire size vs. fire radiative power (FRP in megawatts) for different GFED regions. The error bars represent the 25th and 75th quantiles of the FS distribution. The colour of the dots and error bars represents the mean burn date of fire patches in each FRP bin. The black line shows the interpolated four-degree polynomial used to smooth the value of FRP associated with maximum median fire size. The background histograms represent the number of fire patches in each FRP bins.

perience higher median fire sizes with a humped shape FS–FRP relationship, while forested areas experience a more linear relationship.

For $1° \times 1°$ cells at global scale, Fig. 4 shows the month with the largest median FS, the month with the highest median FRP and the phase shift between these two months. For most African cells, the month with highest median FRP is shifted between 3 and 6 months after the month with the highest FS. These cells correspond to the regions where high BA (Fig. 1, Giglio et al., 2013) and a high density of fire patches are detected (Laurent et al., 2018). A narrower shift is observed in SEAS, northern AUST and in the cells of South America with a slightly lower number of fire patches and lower BA. In North America (BONA and TENA), BOAS, and central and south AUST, no shift is observed, which means that the largest fires and the most intense fires happened concomitantly during the fire season. Some cells (mainly in Sahel and eastern BOAS–CEAS) displayed a negative shift, meaning that the most intense fires happened sooner than the largest fires.

The global maps of power-law slope parameters β_{begin}, β_{middle} and β_{end} (respectively for the beginning, middle and end of the fire season) are displayed in Fig. 5. The β parameters are only computed when more than 10 fire patches are available during the considered period to ensure a sufficient number of patches in the fit. The differences between β_{end} and β_{begin} are also shown in Fig. 5. The highest β values (β_{begin}, β_{middle} and β_{end}) were mainly obtained in NHAF, northern SHAF, NHSA, SHSA and SEAS, as observed in previous fire size distribution analysis (Hantson et al., 2015; Laurent et al., 2018). In these regions, we found that the value of β is higher at the end of the fire season than at the beginning, meaning that the proportion of small fires rises through the fire season, supporting our early results that the late fire season does not become larger with increasing FRP. In AUST, the β value remains constant all throughout the fire season and increases in eastern BONA, TENA and BOAS, suggesting that later season fires are more dominated by larger fires. For other regions, the limited number of fire patches render the interpretation of the evolution of β through the fire season difficult.

4 Discussion

Following the hypothesis from Rothermel's equation of fire spread, and considering that FRP can be used as a proxy of

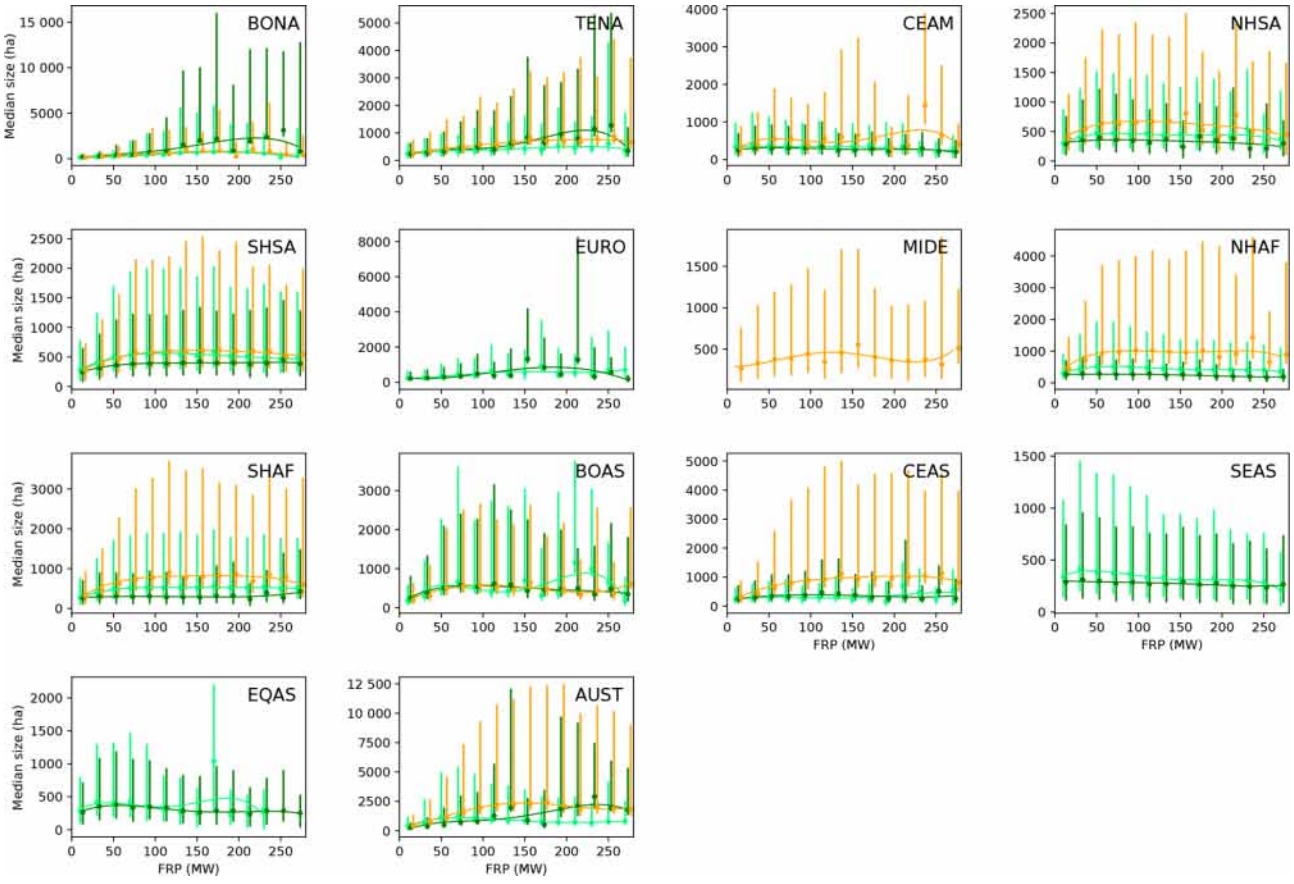

Figure 3. Median fire size vs. fire radiative power (FRP) for different GFED regions for savannas (light green), forests (dark green) and grassland/shrubland (orange). These vegetation classes are obtained by grouping similar land cover type from MODIS Land Cover data, and their spatial extent can be found in the Supplement. The error bars represent the 25th and 75th quantiles of the FS distribution. The colour lines show the interpolated four-degree polynomial used to smooth the value of FRP associated with maximum median fire size for each land cover type.

fire reaction intensity (Wooster et al., 2003, 2005), we used the global fire patch database FRY to test if high FRP fires propagate faster and are therefore systematically larger than low FRP fires. We found that this hypothesis is actually verified for low to intermediate FRP in most fire regions and for the three defined vegetation types. We identified biome-specific FRP vs. FS relationships, with FRP leading to maximum FS being higher in temperate and boreal forests, followed by grasslands, savannas and tropical forests.

In most fire-prone biomes, the positive relationship between FS and FRP does not hold for larger and more intense fire patches (Fig. 2), generally occurring later in the fire season, as previously observed in Australia (Oliveira et al., 2015b). This effect could be explained as follows: at the beginning of the fire season, when the fuel moisture content is still high, FRP is limited as energy is consumed by fuel moisture vaporisation (Alexander, 1982; Pyne et al., 1996), and consequently rate of spread and fire size also become limited. As the fuel becomes drier throughout the fire season (Sow et al., 2013; Sedano and Randerson, 2014; N'Dri et al., 2018), fires become more intense and potentially propagate further. However, the propagation of larger fires can hit some limits due to the fragmentation of the fuel matrix, from intrinsic anthropogenic fragmentation, roads or grazing fields. The barriers limit FS as fires became larger throughout the fire season: these large fires will have a high propensity to reach these barriers. As a result, in fire regions with fragmented vegetation such as African savannas, South East Asia or at the interface between the amazon forest and croplands of South America, a maximum mean FS is reached at intermediate FRP (Fig. 2). The FRP threshold differs, however, between these regions, possibly because their level of landscape fragmentation is different (Taubert et al., 2018).

If fire size would only be limited by the intrinsic structure of vegetation, we would not expect to see the decrease in the proportion of large fires toward the end of the fire season in fire-prone ecosystems (Fig. 5). If the number of individual fire events is already high at the beginning of the fire season, the landscape becomes even more and more fragmented by BA scars (Oliveira et al., 2015a) and fuel load

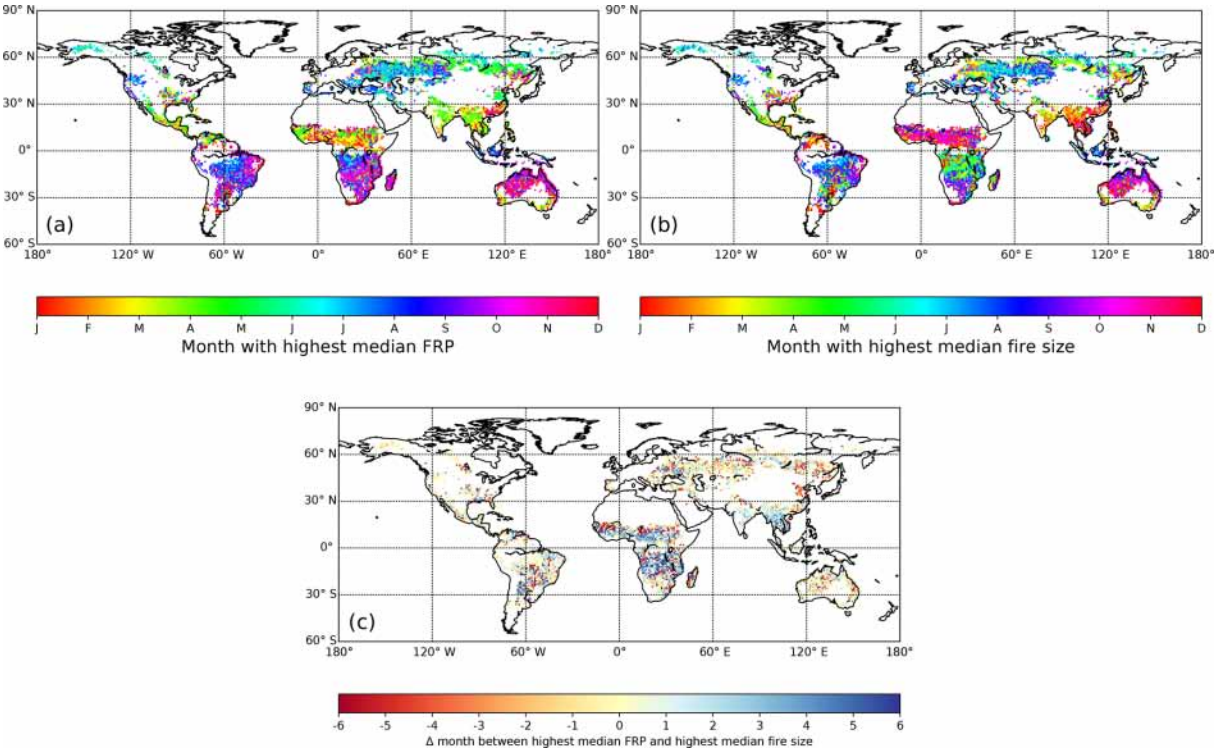

Figure 4. Month with the highest median fire radiative power (FRP, **a**), highest median FS (**b**) and the difference between the two (**c**). In blue cells, the month with the largest fire events happens before the month with the most intense fires. In red cells, the month with the largest fire events happens before the month with the most intense fires. In yellow cells, the months with the largest fires and with the most intense fires are the same.

decrease (N'Dri et al., 2018), meaning that the limitation of fire size due to landscape fragmentation will be higher for fires ignited later in the fire season (Teske et al., 2012). As a consequence, this mechanism may explain why the correlation between FRP and FS becomes negative in Fig. 2 during the late fire season in NHAF, NHSA, CEAM, EQAS, and SEAS and why β_{end} is higher than β_{begin}. This limitation of fire size for intense fires in those regions, possibly due to the feedback between fire and fuel connectivity at the landscape level, is in line with the results obtained from Mondal and Sukumar (2016) relating the effects of recent past fires on fire hazard in dry tropical forests and otherwise theoretically approached from the percolation model applied to wildfires by Archibald et al. (2012). This model shows that the amount of BA is maximised when both the fire spread probability and the fuel matrix connectivity are high. BA dramatically drops if fire spread probability is too low (such as in the beginning of the fire season) or if the fuel array connectivity becomes too small (such as in the end of the fire season). Particularly, the percolation model shows that BA can drop dramatically once 50 %–60 % of the available fuel has burned, which is close to the maximum percentage of BA detected by both MCD64A1 and FireCCI41 products (Giglio et al., 2013; Chuvieco et al., 2016). The IFOI hypothesis, proposed by Luo et al. (2017) to explain why fire occurrence is limited by fire intensity, can be interpreted as a direct consequence of percolation theory applied to fire-prone ecosystems.

For regions where fire events are less frequent, such as in BONA, TENA and EURO (Fig. 2), there is no significant limitation of fire spread and fire size, suggesting that the fragmentation of landscape either from land use or from early season burn scars does not limit fire spread (Owen et al., 2012). Fire size remains positively correlated with fire intensity all throughout the fire season. Moreover, the 75th quantiles for BONA and TENA are higher than for tropical regions (except AUST), most probably because tree species in BONA and TENA (e.g. spruce) are more flammable because crown fires are more frequent and because these ecosystems experience an actual drought period compared to the tropics where rainfall occurs more frequently. They can therefore propagate further than herbaceous fires, hardly turning into crown fires in savannas and woodlands in semi-arid tropical regions. In BOAS the relationship between FS and FRP is different from the one observed in BONA and TENA. This could be a result from the less-flammable vegetation and the highest number of ground fires in BOAS (Kasischke and Bruhwiler, 2003). Moreover, BA detection of surface fires (and consequently, fire patch characterisation) is known to be difficult in boreal Asia, and numerous discrepancies have been observed between the BA products obtained

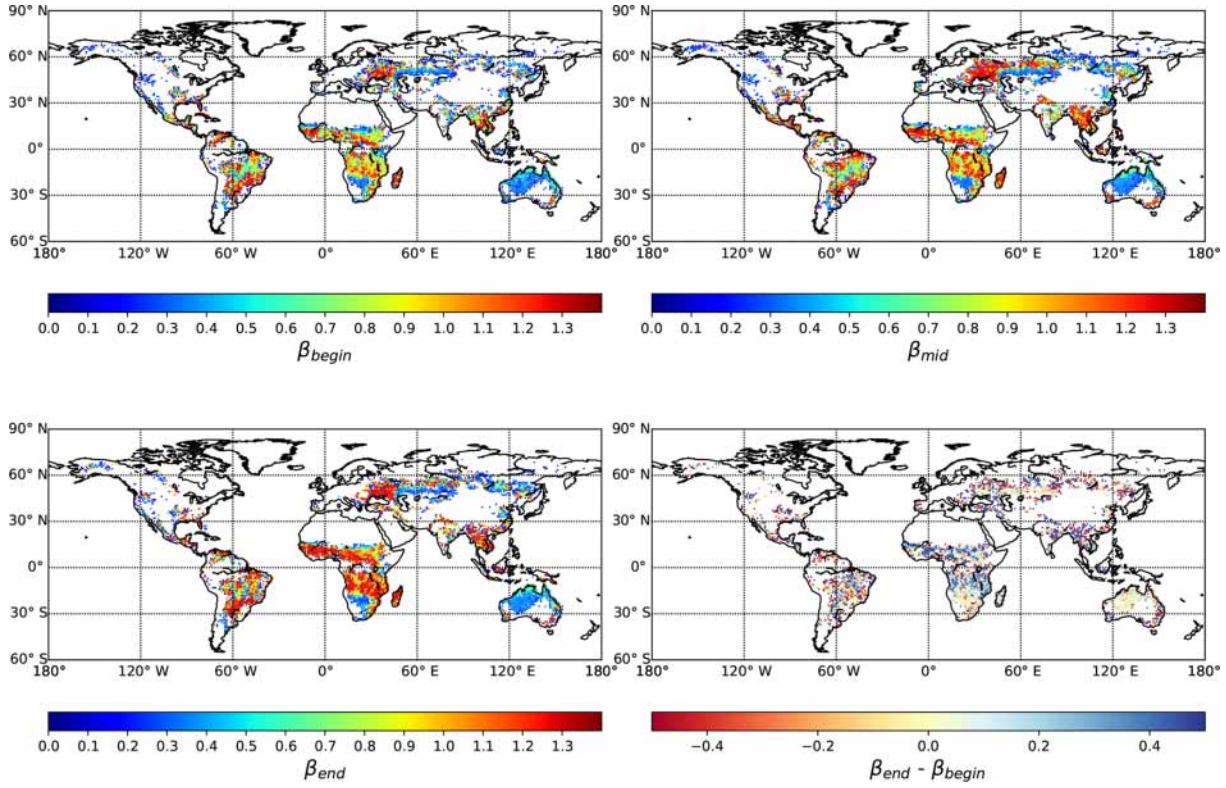

Figure 5. Value of the log-log scale slope of the fire size distribution at the beginning of the fire season, beta (4 months before the month with the highest amount of BA), in the middle of the fire season (corresponding to the month with the highest BA) and at the end of the fire season (4 months after the month with highest BA).

from different moderation resolution sensors (Chuvieco et al., 2016).

The median FS is globally lower for the datasets generated from FRY with smaller cut-off values (see Figs. S1 and S2 in the Supplement) because big fire patches tend to be split into smaller patches for lower cut-off values, reducing the average fire patch size. The median FS is also lower for the FireCCI41-derived datasets due to its ability to detect smaller patches from its better spatial resolution. Changing the survey or the cut-off value does not impact the global distribution of large and small fire patches. Reducing the cut-off to 3 days does not change the observed relationship between FS and FRP. The results obtained from the dataset derived from FireCCI41 follow the same trend, but for some GFED regions (TENA, EURO, NHSA, AUST), the seasonality is shifted 1 month later than for MCD64A1. Reducing the cut-off values lowers the temporal shift observed in Fig. 4 at a global scale (Figs. S3 and S4 in the Supplement), but the global distribution of the shift is conserved. Similarly, FireCCI41 yields smaller shifts than for MCD64A1, but with the same spatial distribution.

In the previous section, we hypothesised that FRP can be used as a proxy of fire reaction intensity but the limitations of such an approach should be mentioned. First, the energy released by a wildfire can be decomposed in three parts: convection, conduction and radiation. FRP only represents the radiative part of the energy released by a fire. Moreover, the fire reaction intensity used in Rothermel's equation does not share the same spatial extent as FRP: fire reaction intensity pertains to the flaming front of the fire, while FRP integrates all the radiative energy emitted over a 1 km^2 window. This means that radiation emitted from smouldering can also contribute to FRP, not only the flaming front. The impact should differ for different wetness conditions and vegetation types: smouldering fires are more frequent in forested areas, whereas in grasslands most of the detected radiative power will be released by the active fire front. Another issue appears from the integration of radiative energy over the 1 km^2 window: very often active burning fire lines do not cover the whole 1 km^2 area so that measured FRP is a mixed signal from both active-burning and unburned areas. However, we can expect this effect to be mitigated by the fact that our analysis does not account for very small fires since the FRY database does not provide fire patches smaller than 107 ha for MCD64A1. Finally, a recent study (Roberts et al., 2018) used 3-D radiative transfer simulations to show that the canopy structure intercepts part of the FRP emitted by surface fires. This means that the FRP measured from remote sensing for forested areas and savannas could underestimate the actual FRP. We can also expect this underestima-

tion to vary with tree species that are associated with different fire regimes. For example, it is probable that the amount of radiation energy intercepted by the canopy differs strongly between crown fires from highly flammable black spruce and jack pine forests from BONA (Rogers et al., 2015) and surface fires from larch-dominated forests in BOAS. These facts advocate the importance of differentiating the relationships between fire size and FRP in different vegetation types with different fire regime and fire adaptations due to varying degrees of reliability of using FRP as a proxy of fire reaction intensity.

Thresholds of FRP detection vary between 9 and 11 MW (Roberts and Wooster, 2008; Schroeder et al., 2010) for the MODIS FRP products, below which reliable detection becomes impossible. In turn, analysis based on comparison with finer-resolution remote-sensing products actually concluded that MODIS might underestimate the number of captured fire pixels by 20 %, particularly for small fires (Wooster et al., 2012; Peterson et al., 2013). This 9–11 MW threshold falls in the first bin of the FRP histograms in Fig. 2 and could therefore explain the peak of the number of fire patches at intermediate FRP ($\sim$ 20–30 MW). The amount of radiative energy reaching the MODIS instruments is much smaller at larger scan angles than at nadir. This means that the MODIS instruments will be less sensitive to low values of FRP at high latitude (Giglio et al., 2003; Schroeder et al., 2005). This could explain the difference of the distribution of FRP associated with fire patches in BONA: the stronger asymmetry of the distribution in this region (i.e. the larger tail toward high FRP values) could arise from missing active fire data from less intense fires in this region. The temporal sampling of FRP also differs with the latitudinal coordinate since the number of satellite overpasses is larger at high latitude than at the Equator (from two observations per day to 15 at the poles; Giglio et al., 2006). This should raise the chance to recover FRP information for fire patches at high latitude, assuming that radiative intensity is high enough to exceed the higher detection threshold at larger scan angles. Also, in some regions (such as NHAF and SHAF), fires exhibit a strong diurnal cycle (Giglio et al., 2006). The detection rate of active fires will therefore be higher if the peak of diurnal intensity is synchronised with satellite overpass. However, we can expect the sampling error rate and the variation in FRP sensitivity with latitude to be more homogeneous within each GFED region than at a global scale.

Fire season length has changed over the last 50 years and is now longer in 25 % of regions of the world (Jolly et al., 2015). An increase in drought intensity in fire-prone environments could yield more intense fire events, yielding larger BA patches for each fire event. However, if the progressive fragmentation of landscape through the fire season limits fire size, then it can be expected that a longer fire season would only have a limited impact on the increase in BA in these regions. In the same way but on a longer timescale in less fire-prone regions, previous large fires have been shown to limit FS in the recent time frame in the western US (Haire et al., 2013), and previous landscape biomass composition, as a result of fire history, is a major factor affecting fire severity in boreal forests (Whitman et al., 2018). Conversely, in regions where the quasi-linear relationship between fire size and FRP is valid even for high FRP, a longer fire season could dramatically increase BA, particularly in North American forests (Gillett et al., 2004; Turetsky et al., 2011). This hypothesis does not account for the impact of increased severity of fire damage to the vegetation in these ecosystems and its feedback on fire propagation and occurrence. Our results are consistent with those of Andela et al. (2017), who showed that, contrary to what would be expected from the rise of the fire danger index, BA tends to decline at a global scale (25 % loss between 1998 and 2015). This decline is especially strong in savannas and grasslands, because of agricultural expansion, which results in a reduction of burnable area and a more fragmented landscape (Kamusoko and Aniya, 2007; Oliveira et al., 2017; Sulieman et al., 2018). Landscape fragmentation is also a tool used for fire management. Indigenous burning practices in West Africa promote early burning and therefore landscape fragmentation in order to limit large and intense fire events which could occur at the end of the fire season (Laris, 2002; Laris and Wardell, 2006; Le Page et al., 2015; Archibald, 2016). Similarly, US forest services used artificial fuel breaks to fragment the landscape and limit fire size (Green, 1977; Agee et al., 2000) as well as fire intensity (Ager et al., 2017).

Some DGVM fire modules explicitly simulate BA as the product of individual successful fire ignitions with mean fire size (Thonicke et al., 2010; Yue et al., 2014). In these models, fire size usually depends on wind speed, fuel bulk density and fuel load. Because of the reduction of the available fuel load due to burning by preceding fires, we can expect than BA saturates toward the end of the drought season in DGVMs, but this mechanism does not account for landscape fragmentation (due either to land use fragmentation or progressive fragmentation by fires). LPJ-LMFire v1.0 (Pfeiffer et al., 2013), a modified version of the Spitfire module for pre-industrial global biomass burning, accounted for passive fire suppression due to landscape fragmentation. Further refining of process-based fire modules would require extensive comparison with fire patch data rather than raw BA.

5 Conclusion

We characterised, for the first time, the actual relationship between fire size and fire intensity using a combination of fire patch size and active fire datasets at a global scale. We found that in most fire-prone ecosystems, fire size increases with fire intensity only at low fire intensity, reaches a threshold at intermediate intensity and then starts to decrease. Conversely, in temperate and boreal forests, FS and FRP are proportional even for high fire intensity. This behaviour

is observed with significant differences among land cover types (shrublands/grasslands, savannas and forests) for both MCD64A1 and FireCCI41 products, and for all cut-off values used for fire patch reconstruction. We suggested that the FRP threshold value is influenced by the fragmentation of the landscape and the feedback between fuel connectivity and BA during the fire season. This fragmentation hypothesis is consistent with the percolation theory applied to fire spread. The fragmentation hypothesis should be further tested with higher-resolution BA datasets, combined with fine-temporal-resolution land cover datasets characterising the landscape fragmentation, associated with temporally varying fuel moisture data, and further considered in the development of fire DGVM models. Additional information such as fire shape complexity and elongation from the FRY database should provide substantial information to support our conclusions.

Data availability. Data are available on the OSU OREME web site (https://data.oreme.org/fire/fire_data, last access: 17 January 2019) (OSU OREME, 2019) or through the DOI: https://doi.org/10.15148/0e999ffc-e220-41ac-ac85-76e92ecd0320.

Supplement. The supplement related to this article is available online at: https://doi.org/10.5194/bg-16-275-2019-supplement.

Author contributions. All authors designed the study and interpreted the results. PL performed the data processing and analysis. PL and FM led the writing of the paper and all authors provided their comments and suggestions.

Competing interests. The authors declare that they have no conflict of interest.

Acknowledgements. Pierre Laurent's post doc grant was supported by the ESA Fire_cci project. Maria Vanesa Moreno's post doc grant was supported by the UM Post-Doc program and University of Montpellier (France) and was co-financed by the ESA Fire_cci project. We also thank OSU OREME for financial support in the "Fire" observation task and for hosting the dataset (https://data.oreme.org/fire/fire_data).

Edited by: Akihiko Ito
Reviewed by: three anonymous referees

References

Agee, J. K, Bahro, B., Finney, M. A., Omi, P. N., Sapsis, D. B., Skinner, C. N., van Wagtendonk, J. W., and Weatherspoon, C. P.: The use of shaded fuelbreaks in landscape fire management, Forest Ecol. Manag., 127, 55–66, 2000.

Ager, A. A., Barros, A. M. G., Preisler, H. K., Day, M. A., Spies, T. A., Bailey, J. D., and Bolte, J. P: Effects of accelerated wilfire on future fire regimes and implications for the United States federal fire policy, Ecol. Soc., 22, 12, https://doi.org/10.5751/ES-09680-220412, 2017.

Alexander, M. E.: Calculating and interpreting forest fire intensities, Can. J. Bot., 60, 349–357, 1982.

Andela, N., Morton, D. C., Giglio, L., Chen, Y., van der Werf, G. R., Kasibhatla, P. S., DeFries, R. S., Collatz, G. J., Hantson, S., Kloster, S., Bachelet, D., Forrest, M., Lasslop, G., Li, F., Mangeon, S., Melton, J. R., Yue, C., and Randerson, J. T.: A human-driven decline in global burned area, Science, 356, 1356–1362, https://doi.org/10.1126/science.aal4108, 2017.

Aragão, L. E. O. C., Anderson, L. O., Fonseca, M. G., Rosan, T. M., Vedovato, L. B., Wagner, F. H., Silva, C. V. J., Silva Junior, C. H. L., Arai, E., Aguiar, A. P., Barlow, J., Berenguer, E., Deeter, M. N., Domingues, L. G., Gatti, L., Gloor, M., Malhi, Y., Marengo, J. A., Miller, J. B., Phillips, O. L., and Saatchi, S.: 21st Century drought-related fires counteract the decline of Amazon deforestation carbon emissions, Nat. Commun., 9, 536, https://doi.org/10.1038/s41467-017-02771-y, 2018.

Archibald, S. and Roy, D. P.: IEEE International Geosciences and remote sensing symposium, 12–17 July 2009, IGARSS, 1–5, Cape Town, South Africa, https://doi.org/10.1109/IGARSS.2009.5417974, 2009.

Archibald, S., Scholes, R. J., Roy, D. P., Roberts, G., and Boschetti, L.: Southern African fire regimes as revealed by remote sensing, Int. J. Wildland Fire, 19, 861–878, https://doi.org/10.1071/WF10008, 2010.

Archibald, S., Staver, A. C., and Levin, S. A.: Evolution of human-driven fire regimes in Africa, P. Natl. Acad. Sci. USA, 109, 847–852, 2012.

Archibald, S., Lehmann, C. E. R., Gomez-Dans, J. L., and Bradstock, R. A.: Defining pyromes and global syndromes of fire regimes, P. Natl. Acad. Sci. USA, 110, 6442–6447, 2013.

Archibald S.: Managing the human component of fire regimes: lessons from Africa, Philos. T. R. Soc. B, 371, 20150346, https://doi.org/10.1098/rstb.2015.0346, 2016.

Baker, W. L.: Restoration of Landscape Structure Altered by Fire Suppression, Conserv. Biol., 8, 763–769, https://doi.org/10.1046/j.1523-1739.1994.08030763.x, 1994.

Barrett, K. and Kasischke, E. S.: Controls on variations in MODIS fire radiative power in Alaskan boreal forests: Implications for fire severity conditions, Remote Sens. Environ., 130, 171–181, https://doi.org/10.1016/j.rse.2012.11.017, 2013.

Bond, W. J. and Keeley, J. E.: Fire as a global "herbivore": The ecology and evolution of flammable ecosystems, Trends Ecol. Evol., 20, 387–394, 2005.

Bowman, D. M. J. S. and Balch, J. K.: Fire in the Earth System, Science, 324, 481–484, 2009.

Cary, G. J., Keane, R. E., Gardner, R. H., Lavorel, S., Flannigan, M. D., Davies, I. D., Li, C., Lenihan, J. M., Rupp, T. S., and Mouillot, F.: Comparison of the sensitivity of landscape-fire-succession models to variation in terrain, fuel pattern, climate and weather, Landsc. Ecol. Eng., 21, 121–137, 2006.

Cary, G. J., Flannigan, M. D., Keane, R. E., Bradstock, R. A., Davies, I. D., Lenihan, J. M., Li, C., Logan, K. A., and Parsons, R. A.: Relative importance of fuel management, ignition management and weather for area burned: evidence from five land-

scape fire succession models, Int. J. Wildland Fire, 18, 147–156, 2009.

Channan, S., Collins, K., and Emanuel, W. R.: Global mosaics of the standard MODIS land cover type data, University of Maryland and the Pacific Northwest National Laboratory, College Park, Maryland, USA, 2014.

Chuvieco, E., Yue, C., Heil, A., Mouillot, F., Alonso-Cansas, I., Padilla, M, Pereira, J. M., Oom, D., and Tansey, K. : A new global burned area product for climate assessment of fire impacts: A new global burned area product. Global. Ecol. Biogeogr., 25, 619–629, 2016.

Flannigan, M. D., Krawchuk, M. A., de Groot, W. J., Wotton, B. M., and Gowman, L. M.: Implications of changing climate for global wildland fire, Int. J. Wildland Fire, 18, 483–507, 2009.

GCOS: Supplemental details to the satellite-based component of the "Implementation Plan for the Global Observing System for Climate in Support of the UNFCCC (2010 Update)", World Meteorological Organization, 154, available at: http://cci.esa.int/sites/default/files/gcos-154.pdf (last access: 15 January 2019), 2011.

Gillett, N. P., Weaver, A. J., Zwiers, F. W., and Flannigan, M. D.: Detecting the effect of climate change on Canadian forest fires, Geophys. Res. Lett., 31, L18211, https://doi.org/10.1029/2004GL020876, 2004.

Giglio, L., Descloitres, J., Justice, C. O., and Kaufman, Y. J.: An enhanced contextual fire detection algorithm for MODIS, Remote Sens. Environ., 87, 273–282, 2003.

Giglio, L., Csiszar, I., and Justice, C. O.: Global distribution and seasonality of active fires as observed with the Terra and Aqua MODIS sensors. J. Geophys. Res., 111, G02016, https://doi.org/10.1029/2005JG000142, 2006.

Giglio, L., Randerson, J. T., and van der Werf, G. R.: Analysis of daily, monthly, and annual burned area using the fourth-generation global fire emissions database (GFED4): Analysis Of Burned Area, J. Geophys. Res.-Biogeo., 118, 317–328, 2013.

Giglio, L., Schroeder, W., and Justice, C.: The collection 6 MODIS active fire detection algorithm and fire products, Remote Sens. Environ., 178, 31–41, 2016.

Green, L.: Fuelbreaks and other fuel modification for wildland fire control, Agricultural Handbook No. 499, 1977.

Greene, D. F., Macdonald, S. E., Cumming, S., and Swift, L.: Seedbed variation from the interior through the edge of a large wildfire in alberta, Can. J. Forest. Res., 35, 1640–1647, 2005.

Haire, S. L., McGarigal, K., and Miller, C.: Wilderness shapes contemporary fire size distributions across landscapes of the western United States, Ecosphere, 4, UNSP15, https://doi.org/10.1890/ES12-00257.1, 2013.

Hantson, S., Pueyo, S., and Chuvieco, E.: Global fire size distribution is driven by human impact and climate: Spatial trends in global fire size distribution, Global Ecol. Biogeogr., 24, 77–86, 2015.

Hantson, S., Arneth, A., Harrison, S. P., Kelley, D. I., Prentice, I. C., Rabin, S. S., Archibald, S., Mouillot, F., Arnold, S. R., Artaxo, P., Bachelet, D., Ciais, P., Forrest, M., Friedlingstein, P., Hickler, T., Kaplan, J. O., Kloster, S., Knorr, W., Lasslop, G., Li, F., Mangeon, S., Melton, J. R., Meyn, A., Sitch, S., Spessa, A., van der Werf, G. R., Voulgarakis, A., and Yue, C.: The status and challenge of global fire modelling, Biogeosciences, 13, 3359–3375, https://doi.org/10.5194/bg-13-3359-2016, 2016.

Hernandez, C., Keribin, C., Drobinski, P., and Turquety, S.: Statistical modelling of wildfire size and intensity: a step toward meteorological forecasting of summer extreme fire risk, Ann. Geophys., 33, 1495–1506, https://doi.org/10.5194/angeo-33-1495-2015, 2015.

Ichoku, C., Giglio, L., Wooster, M. J., and Remer, L. A.: Global characterization of biomass-burning patterns using satellite measurements of fire radiative energy, Remote Sens. Environ., 112, 2950–2962, 2008.

Jolly, W. M., Cochrane, M. A., Freeborn, P. H., Holden, Z. A., Brown, T. J., Williamson, G. J., and Bowman, D. M. J. S.: Climate-induced variations in global wildfire danger from 1979 to 2013, Nat. Commun., 6, 7537, https://doi.org/10.1038/ncomms8537, 2015.

Kamusoko C. and Aniya M.: Land use/cover change and landscape fragmentation analysis in the Bindura District, Zimbabwe, Land Degrad. Dev., 18, 221–223, 2007.

Kasischke, E. S. and Bruhwiler, L. P.: Emissions of carbon dioxide, carbon monoxide and methane from boreal forest fires in 1998, J. Geophys. Res., 108, 8146, https://doi.org/10.1029/2001JD000461, 2003.

Krawchuk, M. A., Moritz, M. A., Parisien, M.-A., Van Dorn, J., and Hayhoe, K.: Global pyrogeography: The current and future distribution of wildfire, PLoS One, 4, e5102, https://doi.org/10.1371/journal.pone.0005102, 2009.

Laris, P.: Burning the seasonal mosaic: preventative burning strategies in the wooded savanna of southern Mali, Hum. Ecol., 30, 155–186, https://doi.org/10.1023/A:1015685529180, 2002.

Laris, P. and Wardell, D. A.: Good, bad or "necessary evil"? Reinterpreting the colonial burning experiments in the savanna landscapes of West Africa, Geogr. J., 172, 271–290, 2006.

Laurent, P., Mouillot, F., Yue, C., Ciais, P., Moreno, M. V., and Nogueira, J. M. P.: FRY, a global database of fire patch functional traits derived from space-borne burned area products, Sci. Data, 5, 180132 https://doi.org/10.1038/sdata.2018.132, 2018.

Le Page, Y., Morton, D., Bond-Lamberty, B., Pereira, J. M. C., and Hurtt, G.: HESFIRE: a global fire model to explore the role of anthropogenic and weather drivers, Biogeosciences, 12, 887–903, https://doi.org/10.5194/bg-12-887-2015, 2015.

Luo, R., Hui, D., Miao, N., Liang, C., and Wells, N.: Global relationship of fire occurrence and fire intensity: A test of intermediate fire occurrence-intensity hypothesis: Fire Occurrence-Intensity Relationship, J. Geophys. Res.-Biogeo., 122, 1123–1136, 2017.

Mondal, N. and Sukumar, R.: Fires in seasonnaly dry tropical forest: testing the varying constraints hypothesis acriss a regional rainfall gradient, PLoS One, 11, e0159691, https://doi.org/10.1371/journal.pone.0159691, 2016.

Mouillot, F., Schultz, M. G., Yue, C., Cadule, P., Tansey, K., Ciais, P., and Chuvieco, E.: Ten years of global burned area products from spaceborne remote sensing – A review: Analysis of user needs and recommendations for future developments, Int. J. Appl. Earth Obs., 26, 64–79, 2014.

N'Dri, A. B., Soro, T. D., Gignoux J., Dosso, K., Kone, M., N'Dri, J. K., Kone, N. A., and Barot, S.: Season affects fire behaviour in annually burned humid savannah of west Africa, Fire Ecol., 14, UNSP5, https://doi.org/10.1186/s42408-018-0005-9, 2018.

Nogueira, J. M. P., Ruffault, J., Chuvieco, E., and Mouillot, F.: Can we go beyond burned area in the assessment of global remote

sensing products with fire patch metrics?, Remote Sens., 9, 7, https://doi.org/10.3390/rs9010007, 2017.

Oliveira, S. L. J., Campagnolo, M. L., Owen, P., Edwards, A. C., Russel-Smith, J., and Pereira, J. M. C.: Ecological Implications of Fine-Scale Fire Patchiness and Severity in Tropical Savannas of Northern Australia, Fire Ecol., 11, 10–31, 2015a.

Oliveira, S. L. J., Maier, S. W., Pereira, J. M. C., and Russell-Smith, J.: Seasonal differences in fire activity and intensity in tropical savannas of northern Australia using satellite measurments of fire radiative power, Int. J. Wildland Fire, 24, 249–260, 2015b.

Oliveira, S. N., de Carvalho, O. A., Gomes, R. A. T., Guimaraes, R. F., and McManus, C. M.: Landscape-fragmentation change due to recent agricultural expansion in the Brazilian Savanna, Western Bahia, Brazil, Reg. Environ. Change, 17, 411–423, 2017.

OSU OREME: Fire data, available at: https://data.oreme.org/fire/fire_data, last access: 17 January 2019.

Owen, F. P., Russel-Smith, J., and Watt, F.: The influence of prescribed fire on the extent of wildfire in savanna landscapes of western Arnhem Land, Australia, Int. J. Wildland Fire., 21, 297–305, 2012.

Pausas, J. G. and Ribeiro, E.: The global fire-productivity relationship, Global Ecol. Biogeogr., 22, 728–736, 2013.

Peterson, D., Wang, J., Ichoku, C., Hyer, E., and Ambrosia, V.: A sub pixel calculation of fire radiative power from MODIS observations: 1 algorithm development and initial assessment, Remote Sens. Environ., 129, 262–279, 2013.

Pfeiffer, M., Spessa, A., and Kaplan, J. O.: A model for global biomass burning in preindustrial time: LPJ-LMfire (v1.0), Geosci. Model Dev., 6, 643–685, https://doi.org/10.5194/gmd-6-643-2013, 2013.

Pyne, S. J, Andrews, P. L., and Laven, R. D.: Introduction to Wildland Fire, Wiley, Hoboken, NJ, USA, 1996.

Rabin, S. S., Melton, J. R., Lasslop, G., Bachelet, D., Forrest, M., Hantson, S., Kaplan, J. O., Li, F., Mangeon, S., Ward, D. S., Yue, C., Arora, V. K., Hickler, T., Kloster, S., Knorr, W., Nieradzik, L., Spessa, A., Folberth, G. A., Sheehan, T., Voulgarakis, A., Kelley, D. I., Prentice, I. C., Sitch, S., Harrison, S., and Arneth, A.: The Fire Modeling Intercomparison Project (FireMIP), phase 1: experimental and analytical protocols with detailed model descriptions, Geosci. Model Dev., 10, 1175–1197, https://doi.org/10.5194/gmd-10-1175-2017, 2017.

Roberts, G. and Wooster, M. J.: Fire Detection and Fire Characterization over Africa using Meteosat SEVIRI, IEEE Trans. Geosci. Remote, 48, 1200–1219, 2008.

Roberts, G., Wooster M. J., Perry G. L., and Drake, N.: Retrieval of biomass combustion rates and totals from fire radiative power observations: application to southern Africa using geostationary SEVIRI imagery, J. Geophys. Res., 100, D21111, https://doi.org/10.1029/2005JD006018, 2005.

Roberts, G., Wooster, M. J., Lauret, N., Gastellu-Etchegorry, J.-P., Lynham, T., and McRae, D.: Investigating the impact of overlying vegetation canopy structures on fire radiative power (FRP) retrieval through simulation and measurement, Remote Sens. Environ., 217, 158–171, 2018.

Rogers, B. M., Soja, A. J., Goulden, M. L., and Randerson, J. T.: Influence of tree species on continental differences in boreal fires and climate feedbacks, Nat. Geosci., 8, 228–234, https://doi.org/10.1038/NGEO2352, 2015.

Rothermel, R. C.: A mathematical model for predicting fire spread in wildland fuels, USDA Forest Services, Research Paper, INT-115, 1972.

Schroeder, W., Morisette, J. T., Csiszar, I., Giglio, L., Morton, D., and Justice, C. O.: Characterizing vegetation fire dynamics in Brazil through multisatellite data: Common trends and practical issues, Earth Interact., 9, 1–26, 2005.

Schroeder, W., Csiszar I., Giglio L., and Schmidt C.: On the use of fire radiative power, area, and temperature estimates to characterize biomass burning via moderate to coarse spatial resolution remote sensing data in the Brazilian Amazon, J. Geophys. Res., 115, D21121, https://doi.org/10.1029/2009JD013769, 2010.

Scott, A. C., Bowman, D. M. J. S., Bond, W. J., Pyne, S. J., and Alexander, M. E.: Fire on Earth: An Introduction, Wiley-Blackwell, Hoboken, NJ, USA, 434 pp., 2014.

Sedano, F. and Randerson, J. T.: Multi-scale influence of vapor pressure deficit on fire ignition and spread in boreal forest ecosystems, Biogeosciences, 11, 3739–3755, https://doi.org/10.5194/bg-11-3739-2014, 2014.

Sparks, A. M., Kolden, C. A., Smith, A. M. S., Boschetti, L., Johnson, D. M., and Cochrane, M. A.: Fire intensity impacts on post-fire temperate coniferous forest net primary productivity, Biogeosciences, 15, 1173–1183, https://doi.org/10.5194/bg-15-1173-2018, 2018.

Sow, M., Mbow, C., Hely, C., Fensholt, R., and Sambou, B.: Estimation of herbaceous fuel moisture content using vegetation indices and land surface temperature from MODIS data, Remote Sens., 5, 2617–2638, 2013.

Sulieman, H. M.: Exploring drivers of forest degradation and fragmentation in sudan: the case of Erawashda forest and its surrounding community, Sci. Total Environ., 621, 895–904, 2018.

Tang, W. and Arellano Jr., A. F.: Investigating dominant characteristics of fires across the Amazon during 2005–2014 through satellite data synthesis of combustion signatures, J. Geophys. Res.-Atmos., 122, 1224–1245, https://doi.org/10.1002/2016JD025216, 2017.

Taubert, F., Fischer, R., Groeneveld, J., Lehmann, S., Müller, M. S., Roedig, E., Wiegand, T., and Huth, A.: Global patterns of tropical forest fragmentation, Nature, 554, 519–522, 2018.

Teske, C. C., Seielstad, C. A., and Queen, L. P.: Characterizing fire on fire interactions in three large wilderness areas, Fire Ecol., 8, 82–106, 2012.

Thonicke, K., Spessa, A., Prentice, I. C., Harrison, S. P., Dong, L., and Carmona-Moreno, C.: The influence of vegetation, fire spread and fire behaviour on biomass burning and trace gas emissions: results from a process-based model, Biogeosciences, 7, 1991–2011, https://doi.org/10.5194/bg-7-1991-2010, 2010.

Turetsky, M. R., Kane E. S., Harden, J. W., Ottmar, R. D., Manies, K. L., Hoy, E., and Kasischke, E. S.: Recent acceleration of biomass burning and carbon losses in Alaskan forests and peatlands, Nat. Geosci., 4, 27–31, 2011.

Turner, M. G.: Landscape ecology: the effect of pattern on process, Annu. Rev. Ecol. Syst., 20, 171–197, 1989.

Whitman, E., Parisien, M. A., Thompson, D. K., Hall, R. J., Skakun, R. S., and Flannigan, M. D.: Variability and drivers of burn severity in the northwestern Canadian boreal forest, Ecosphere, 9, e02128, https://doi.org/10.1002/ecs2.2128, 2018.

Wooster, M. J., Roberts, A. F., Perry, G. L. W., and Kaufman, Y. J.: Retrieval of biomass combustion rates and to-

tals from fire radiative power observations: FRP derivation and calibration relationships between biomass consumption and fire radiative energy release, J. Geophys. Res., 110, D24311, https://doi.org/10.1029/2005JD006318, 2005.

Wooster, M. J., Xu, W., and Nightingale, T.: Sentinel-3 SLSTR active fire detection and FRP product: Pre-launch algorithm development and performance evaluation using MODIS and ASTER datasets, Remote Sens. Environ., 120, 236–254, 2012.

Wooster, M. J., Roberts, G., Smith, A. M. S., Johnston, J., Freeborn, P., Amici, S., and Hudak, A. T.: Thermal Remote Sensing of Active Vegetation Fires and Biomass Burning Events, Thermal Infrared Remote Sensing: Sensors, Methods and Applications, edited by: Kuenzer, C. and Dech, S., Springer, the Netherlands, 17, 347–390, 2013.

Yue, C., Ciais, P., Cadule, P., Thonicke, K., Archibald, S., Poulter, B., Hao, W. M., Hantson, S., Mouillot, F., Friedlingstein, P., Maignan, F., and Viovy, N.: Modelling the role of fires in the terrestrial carbon balance by incorporating SPITFIRE into the global vegetation model ORCHIDEE – Part 1: simulating historical global burned area and fire regimes, Geosci. Model Dev., 7, 2747–2767, https://doi.org/10.5194/gmd-7-2747-2014, 2014.